NASA
Technical
Paper
1978

April 1982

Effects of Cable Geometry and Aircraft Attitude on the Accuracy of a Magnetic Leader Cable System for Aircraft Guidance During Rollout and Turnoff

W. Thomas Bundick

NASA

NASA Technical Paper 1978

1982

Effects of Cable Geometry and Aircraft Attitude on the Accuracy of a Magnetic Leader Cable System for Aircraft Guidance During Rollout and Turnoff

W. Thomas Bundick
Langley Research Center
Hampton, Virginia

National Aeronautics and Space Administration

Scientific and Technical Information Branch

SUMMARY

A single-wire magnetic leader cable laid along the path the aircraft is to follow is a potential source of guidance information during rollout, turnoff, and taxi. This report contains a theoretical analysis of the errors produced in such a system by the geometry of the cable layout and by a nonzero aircraft attitude. It was found that neglecting the aircraft attitude in processing the leader cable signals to obtain the aircraft heading can cause significant errors, even for small attitude angles. Displacement from the cable, on the other hand, can be obtained with reasonable accuracy without compensating for aircraft attitude.

Analysis of a rectangular loop geometry for the cable shows that for practical loop widths, a nonlinear calibration curve is required to obtain accurate estimates of aircraft heading and lateral displacement relative to the cable, although a linear approximation may be sufficiently accurate for many applications.

From analysis of a practical runway turnoff geometry, it was found that the errors produced by the turnoff are small for the estimates of displacement and are largest for the estimates of heading at the beginning and end of each turn. The magnitude of the error was not particularly sensitive to the turnoff angle, but the heading error did increase with a decreasing turn radius. In all cases, the errors were minimum at or near the cable.

Although the leader cable concept was originally formulated for the hypothetical case of an infinite straight wire, results of this analysis show that the concept remains viable for a practical closed-loop runway-turnoff-taxiway configuration. Of course, the effect of all leader cable sensor errors on total guidance and control system performance must be evaluated via computer simulation and flight tests.

INTRODUCTION

The new microwave landing system (MLS) being developed by the Federal Aviation Administration is designed to provide sufficiently accurate guidance during final approach and touchdown to permit aircraft to land under conditions of severely reduced visibility. In addition, the azimuth and DME functions of the MLS will provide some guidance during rollout under these same poor visibility conditions. However, guidance during turnoff and taxi is currently available only through visual means and thus is inadequate during periods of extremely low visibility. Furthermore, the MLS, together with advanced avionics and air-traffic-control techniques, has the potential to increase the runway capacity by decreasing the spacing between landing aircraft. Decreased landing intervals demand that runway occupancy time be decreased, that is, that landing aircraft be cleared from the runway rapidly. One technique for reducing runway occupancy time is the use of high-speed turnoffs.

Safe and efficient use of high-speed turnoffs requires the availability of turnoff guidance, particularly for use with automatic controls. Clearly, if the MLS and high-speed turnoffs are to be used to their peak potential, appropriate guidance information during turnoff and taxi must be made available. One potential source of such guidance is the magnetic leader cable. The cable, or wire, would be buried in the runway, turnoff, and taxiway along the path that the aircraft is to follow. (See

fig. 1.) A sensor in the aircraft would detect signals from the cable and provide guidance to the pilot or automatic control system.

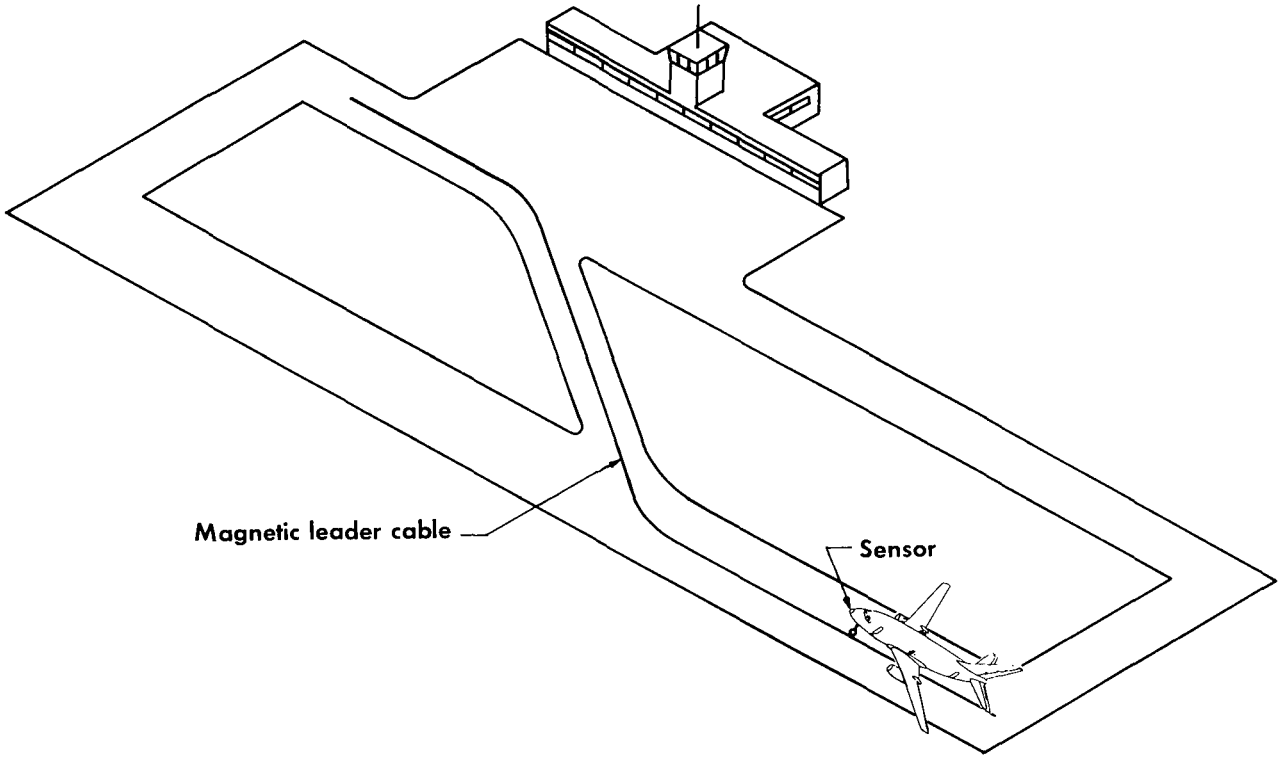

Figure 1.- Rollout and turnoff guidance using a magnetic leader cable.

As early as the 1950's, the magnetic leader cable was investigated by the British (refs. 1 and 2) as a source of guidance during final approach and landing, but it was never adopted as an operational system. One of the factors limiting its usefulness in that application was the difficulty in obtaining accurate guidance during final approach prior to touchdown. This difficulty would be avoided in the present concept by utilizing the system only after touchdown. Other applications considered for the magnetic leader cable include guidance of automobiles (ref. 3) and special-purpose military vehicles (ref. 4).

Work on the magnetic leader cable for aircraft guidance has been revived as part of the NASA Terminal Configured Vehicle (TCV) Program. One facet of this effort involves the investigation via computer simulation of aircraft performance during rollout and turnoff using MLS and magnetic leader-cable sensors. Early portions of this work have been reported in references 5, 6, and 7. A second facet is the development of a magnetic leader cable sensor system. Although two-wire cable configurations have been considered for other applications (ref. 3), a single-wire system was selected for the current application to simplify the task of embedding the cable in the runway and taxiway along the desired path. One part of this development is a theoretical analysis of a practically configured cable and sensor system. Such a theoretical analysis is the subject of this report. Previous analyses have assumed an infinitely long, straight wire; the present analysis investigates the effects of aircraft attitude, a finite loop size, and a typical turnoff geometry on the poten-

tial accuracy of the system. Together with system performance requirements and other data, the results of this analysis can then be used to determine such things as minimum loop width and the need for aircraft attitude compensation.

SYMBOLS

A area of coil, m^2

a_1, a_2, a_3, a_4 intermediate variables used in computation of magnetic intensities $\vec{H}_1$, $\vec{H}_2$, $\vec{H}_3$, and $\vec{H}_4$, respectively (see eqs. (21), (23), (25), and (27)), m^2

$\vec{B}(t)$ magnetic induction field, Wb/m^2

B_x, B_y, B_z Cartesian components of $\vec{B}$, Wb/m^2

d perpendicular displacement from cable in xy-plane, m

$\overrightarrow{d\ell}$ incremental length of current element, m

$\hat{d}_1, \hat{d}_2$ estimate of d defined by equations (18a) and (18b), same as $\hat{y}_1$ and $\hat{y}_2$ before turnoff

G $= \dfrac{\mu_o \omega NAI}{2\pi}$

$\vec{H}$ magnetic intensity, A/m

H_x, H_y, H_z Cartesian components of $\vec{H}$, A/m

$\vec{H}_1, \vec{H}_2, \vec{H}_3, \vec{H}_4$ magnetic intensity produced by current in sides 1, 2, 3, and 4, respectively, of rectangular loop, A/m

I peak current in cable, A

$I(t)$ time-varying current in cable, A

$\hat{i}_x, \hat{i}_y, \hat{i}_z$ unit vectors along Cartesian axes

$\hat{i}_1, \hat{i}_2, \hat{i}_3$ unit vectors perpendicular to planes of coils 1, 2, and 3, respectively

$\vec{i}_\theta$ unit vectors in θ-direction in cylindrical coordinates

L length of cable loop in x-direction, m

L_s length of straight segment of cable between two turns of turnoff, m

L_1 x-coordinate at start of turnoff, m

N number of turns in coil

P point at which magnetic field is calculated

R_1, R_2 radii of first and second turns, respectively, in turnoff, m

$\vec{r}$ radius vector from origin to point P, m

$\vec{r}_c$ vector from current element $I\,\vec{d\ell}$ to point P, m

S surface area, m^2

S_{ep} distance between runway and taxiway, m

s curvilinear distance along path parallel to and at a distance d from cable, m

t time, sec

V_1, V_2, V_3 peak voltage output of coils 1, 2, and 3, respectively, V

V_{y_1} peak voltage at sensor's $\hat{y}_1$ output, zV_3/V_2, V

V'_{y_1} voltage equivalent to V_{y_1} in x',y',z' coordinate system

$v_1(t)$ time-varying voltage output of coil 1, V

W width of cable loop in y-direction, m

x,y,z Cartesian coordinates of point P or of coils

x',y',z' coordinates where x' = -x, y' = -y, and z' = z

x_c, y_c, z_c Cartesian coordinates of cable current element

$\tilde{y}_1, \tilde{y}_2$ estimates of coil displacement from cable defined by equations (17a) and (17b), m

$\hat{y}_1, \hat{y}_2$ estimates of coil displacement from cable defined by equations (18a) and (18b), m

$\hat{\hat{y}}_1$ estimate of coil displacement from cable using nonlinear calibration curve, m

$\hat{\hat{y}}'_1$ estimate equivalent to $\hat{\hat{y}}_1$ in x',y',z' coordinate system

θ, ϕ, ψ angles of pitch, roll, and yaw, respectively (θ also used as angular coordinate in cylindrical coordinates), rad

θ_E turnoff, or exit, angle, rad or deg

μ_o permeability of free space, $4\pi \times 10^{-7}$ Wb/A-m

ρ radial coordinate in cylindrical coordinates, m

$\phi_1(t)$ magnetic flux linking coil 1, Wb

ψ aircraft heading relative to cable (equivalent to yaw during rollout), rad or deg

$\tilde{\psi}$ estimate of ψ defined by equation (17d), rad or deg

$\hat{\psi}$ estimate of ψ defined by equation (18c), rad or deg

ω angular frequency of current in cable, rad/sec

Abbreviations:

DME distance measuring equipment

MLS microwave landing system

TCV terminal configured vehicle

DEVELOPMENT OF THE THEORY

Consider an infinitely long, straight conductor coincident with the x-axis carrying a current I(t), as depicted in figure 2. The magnetic leader cable utilizes a sinusoidal current in the audio frequency range, say 100 Hz to 2500 Hz. Because of the extremely long wavelengths (greater than 100 km) and short distances (less than 5 km) involved, the propagation time can be neglected. Thus in order to simplify the mathematics, the time dependence of the current and of the resulting magnetic field will be suppressed, and the quasi-static approximation will be used in the remainder of this report.

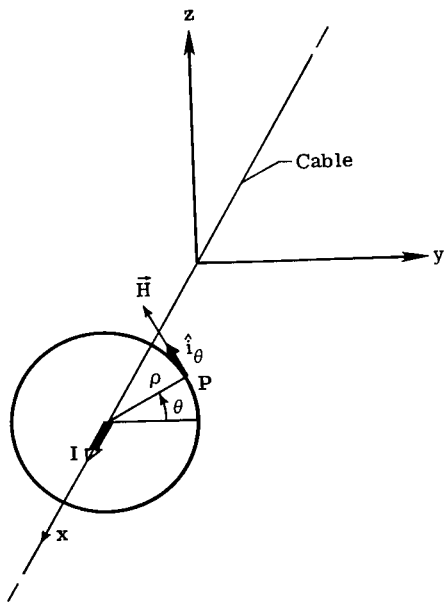

Figure 2.- Geometry for infinite straight cable.

Returning now to figure 2, the magnetic intensity $\vec{H}$ at point P can be computed using Ampere's circuital law as follows:

$$\int_C \vec{H} \cdot \vec{d\ell} = I \tag{1}$$

Because the field is symmetrical about the conductor and is everywhere in the θ-direction, equation (1) simplifies to

$$\vec{H} = \frac{I}{2\pi\rho}\,\hat{i}_\theta \tag{2}$$

In Cartesian coordinates, equation (2) becomes

$$H_x = 0 \tag{3a}$$

$$H_y = -\frac{I}{2\pi}\,\frac{z}{y^2 + z^2} \tag{3b}$$

$$H_z = \frac{I}{2\pi}\,\frac{y}{y^2 + z^2} \tag{3c}$$

Suppose there were three mutually orthogonal coils located at point P such that the axes $\hat{i}_1$, $\hat{i}_2$, and $\hat{i}_3$ of the coils were parallel to the coordinate axis x, y, and z, respectively. From Faraday's law the voltage induced in coil 1 by the magnetic field is

$$v_1(t) = -\frac{d\phi_1(t)}{dt} \tag{4}$$

If coil 1 has number of turns N with area A and the cable current is sinusoidal with angular frequency ω, the flux linkage is given by the integral

$$\phi_1(t) = N \int_{S_1} \vec{B}(t) \cdot \hat{i}_1 \, dS = NAB_x \cos \omega t \tag{5}$$

The voltage induced in coil 1 is then

$$v_1(t) = \omega NAB_x \sin \omega t \tag{6a}$$

or in terms of peak values

$$V_1 = \omega NAB_x = \mu_o \omega NAH_x \tag{6b}$$

Combining equations (3a) and (6b), we see that

$$V_1 = 0 \tag{7a}$$

Similarly for coils 2 and 3, we find that

$$V_2 = - \frac{\mu_o \omega NAI}{2\pi} \frac{z}{y^2 + z^2} \tag{7b}$$

and

$$V_3 = \frac{\mu_o \omega NAI}{2\pi} \frac{y}{y^2 + z^2} \tag{7c}$$

Now take the ratio of voltages V_3 to V_2 and solve for y. Thus,

$$y = - \frac{zV_3}{V_2} \tag{8}$$

If the coil height z is known, then the displacement y of the coils from the magnetic leader cable can be determined by measuring the coil voltages V_2 and V_3 and using equation (8). Note that in this case the displacement y is a linear function of the ratio of voltages V_3/V_2. The displacement y can also be determined via an alternative technique which requires a knowledge of the current I in the cable but which does not require that the height z be known. This can be seen by finding the ratio of V_3 to $V_2^2 + V_3^2$ as follows:

$$\frac{V_3}{V_2^2 + V_3^2} = \frac{2\pi y}{\mu_o \omega INA} \tag{9}$$

Equation (9) can be solved for y to obtain the following:

$$y = \frac{\mu_o \omega INA}{2\pi} \frac{V_3}{V_2^2 + V_3^2} \tag{10}$$

Note that this expression for y is a linear function of the ratio $V_3/(V_2^2 + V_3^2)$.

Suppose now that the coils are rotated in the xy-plane such that $\hat{i}_1$ makes an angle ϕ with the x-axis, as in figure 3. Now the voltage output V_3 of the z-coil remains the same, but (since B_x equals zero) the voltages V_1 and V_2 become

$$V_1 = \omega NAB_y \sin \phi \tag{11a}$$

$$V_2 = \omega NAB_y \cos \phi \tag{11b}$$

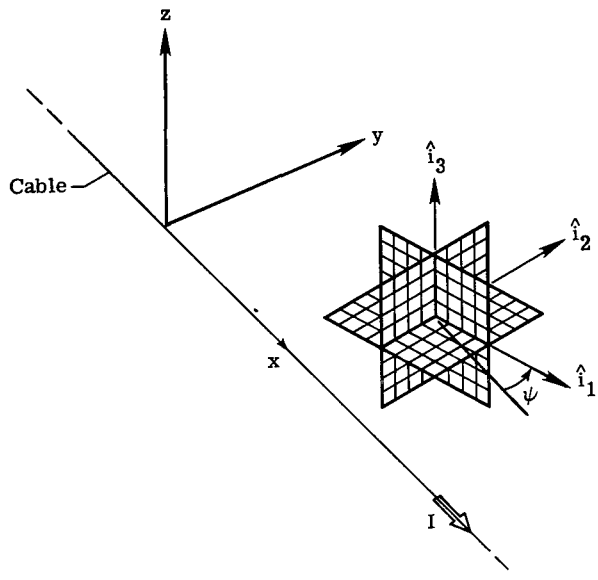

Figure 3.- Coil geometry.

Taking the ratio V_1/V_2, we find that

$$\frac{V_1}{V_2} = \tan \phi \tag{12}$$

Equation (12) can be solved for ϕ to give

$$\phi = \text{arc tan } (V_1/V_2) \tag{13a}$$

which, for small values of ϕ, can be approximated by

$$\phi \approx \frac{V_1}{V_2} \tag{13b}$$

Note that in this approximation ϕ is a linear function of the ratio V_1/V_2. Equation (8) for the displacement now becomes

$$y = - \frac{zV_3 \cos \phi}{V_2} \tag{14}$$

However, if ϕ is small, equation (14) can be approximated by equation (8).

We have shown conceptually that for an infinitely long, straight cable carrying a current I, the lateral displacement y (relative to the cable) of a set of three mutually orthogonal coils can be determined by measuring the voltage output of the appropriate coils and processing these measurements with either of two algorithms.

The use of one algorithm requires that the height of the coils be known, while use of the other algorithm requires that the magnitude of the current in the cable be known. Furthermore, the angle of rotation of the coil in the xy-plane can be determined by using the coil voltages and processing them with a third algorithm. Conceptually it follows that if the coils are rigidly attached to an aircraft and the magnetic cable is laid on the runway center line, the sensor can be used to measure the displacement of the aircraft from the center line and the heading of the aircraft relative to the center line. In the remainder of this report we will examine the effects on system accuracy when the linear relationships developed above are used to process signals in practical situations involving nonzero aircraft attitudes, rectangular loops, and different turnoff geometries.

EFFECTS OF AIRCRAFT ATTITUDE

The previous development has assumed that the z-coil has its axis in the z-direction. With the coils in an aircraft this may not always be true, even when the aircraft is taxiing. Suppose the coils have been rotated through a yaw angle ψ, a pitch angle θ, and a roll angle ϕ, in that order. The voltage outputs of the coils now become

$$\begin{bmatrix} V_1 \\ V_2 \\ V_3 \end{bmatrix} = \omega NA \begin{bmatrix} \cos\theta\cos\psi & \cos\theta\sin\psi & -\sin\theta \\ -\cos\phi\sin\psi + \sin\phi\sin\theta\cos\psi & \cos\phi\cos\psi + \sin\phi\sin\theta\sin\psi & \sin\phi\cos\theta \\ \sin\phi\sin\psi + \cos\phi\sin\theta\cos\psi & -\sin\phi\cos\psi + \cos\phi\sin\theta\sin\psi & \cos\phi\cos\psi \end{bmatrix} \begin{bmatrix} B_x \\ B_y \\ B_z \end{bmatrix} \tag{15a}$$

For small angles, equation (15a) can be approximated by

$$\begin{bmatrix} V_1 \\ V_2 \\ V_3 \end{bmatrix} \approx \omega NA \begin{bmatrix} 1 & \psi & -\theta \\ -\psi & 1 & \phi \\ \theta & \phi & 1 \end{bmatrix} \begin{bmatrix} B_x \\ B_y \\ B_z \end{bmatrix} \tag{15b}$$

Combining equation (15b) with equations (3), the coil voltages are

$$\begin{bmatrix} V_1 \\ V_2 \\ V_3 \end{bmatrix} = G \begin{bmatrix} 1 & \psi & -\theta \\ -\psi & 1 & \phi \\ \theta & -\phi & 1 \end{bmatrix} \begin{bmatrix} 0 \\ \dfrac{-z}{y^2 + z^2} \\ \dfrac{y}{y^2 + z^2} \end{bmatrix} \tag{16}$$

where $G = \dfrac{\mu_o \omega NAI}{2\pi}$.

Equation (16) can be solved for the desired variables y and ϕ:

$$\tilde{y}_1 = \frac{z\left(\phi + \dfrac{V_3}{V_2}\right)}{\dfrac{\phi V_3}{V_2} - 1} \tag{17a}$$

$$\tilde{y}_2 = \frac{G(1 + \phi^2)V_3}{V_2^2 + V_3^2} - \phi z \approx \frac{GV_3}{V_2^2 + V_3^2} - \phi z \tag{17b}$$

$$\tilde{\psi} = \left(1 - \phi \frac{y}{z}\right)\frac{V_1}{V_2} - \theta \frac{y}{z} \tag{17c}$$

The solution for $\tilde{\psi}$ requires a knowledge of y, which is an unknown to be determined. In order to compute $\tilde{\psi}$, use for y the value $\tilde{y}_1$ calculated in equation (17a) - or alternatively $\tilde{y}_2$. Then

$$\tilde{\psi} = \left(1 - \phi \frac{\tilde{y}_1}{z}\right)\frac{V_1}{V_2} - \theta \frac{\tilde{y}_1}{z} \tag{17d}$$

These algorithms (eqs. (17a), (17b), and (17d)), which contain small angle approximations, can be used to compute estimates of the displacement and heading if the aircraft attitude angles θ and ϕ are available.

During rollout, turnoff, and taxi, the aircraft attitude angles should be close to zero. Extreme values for yaw, pitch, and roll probably will not exceed ±10°, ±5°, and ±5°, respectively. Within these limits for the attitude angles, what then are the errors in the estimated displacement and heading introduced by the small-angle approximations in equations (15b) through (17d)? These errors have been computed for several combinations of attitude angles for a coil height of 2.5 m; the errors in $\tilde{y}_1$ and $\tilde{\psi}$ are plotted in figure 4. From figure 4(a) it can be seen that for the attitudes used in computing these results, the errors in $\tilde{y}_1$ produced by the small-angle approximations never exceed 0.39 m for displacements y up to ±30 m. The error in $\tilde{y}_2$ never exceeds 0.05 m and is not plotted. The effects of these errors on the performance of an automatic rollout and turnoff system must be evaluated via simulation and test. However, it is expected that these errors can easily be tolerated. The error in $\tilde{\psi}$ produced by the small-angle approximation is seen from figure 4(b) to be less than 0.6° for all the cases considered and is less than 0.01° for $\psi = \theta = \phi = 1°$. Thus, it would seem that the error in the estimate $\tilde{\psi}$ may be tolerable.

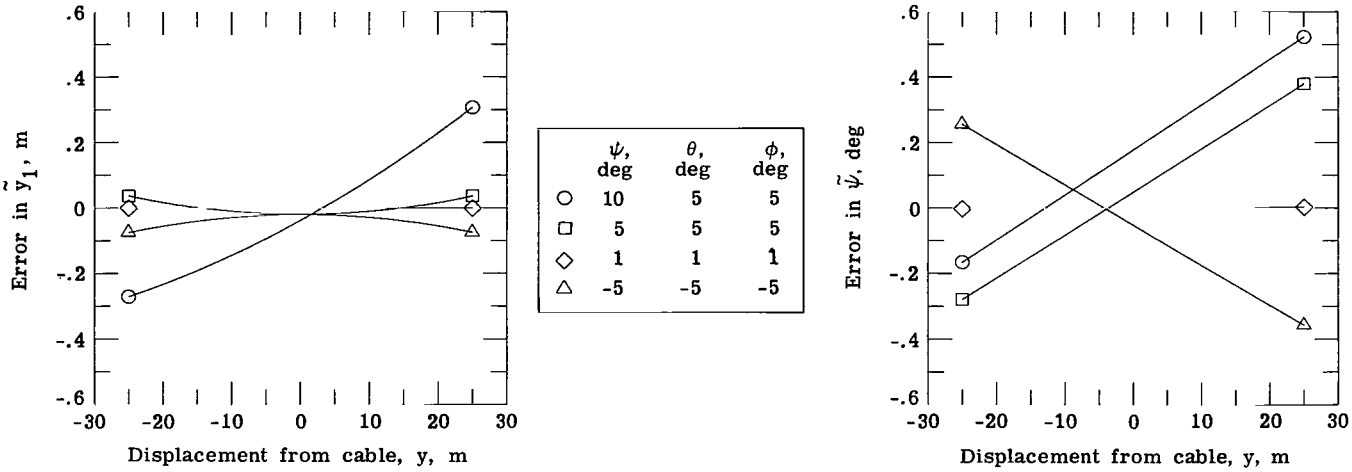

(a) Error in estimate $\tilde{y}_1$.

(b) Error in estimate $\tilde{\psi}$.

Figure 4.- Error in estimates $\tilde{y}_1$ and $\tilde{\psi}$ due to small-angle approximations.

The complexity in instrumentation and computation would be reduced considerably if the aircraft attitude could be ignored, that is, if the displacement and heading could be calculated from the basic algorithms (eqs. (8), (10), and (13b)) as follows:

$$\hat{y}_1 = -\frac{zV_3}{V_2} \tag{18a}$$

$$\hat{y}_2 = \frac{\mu_o \omega NAI}{2\pi} \frac{V_3}{V_2^2 + V_3^2} \tag{18b}$$

$$\hat{\psi} = \frac{V_1}{V_2} \tag{18c}$$

The errors in the estimates computed with these algorithms are plotted for several values of attitude in figure 5. From figure 5(a) the error in $\hat{y}_1$ is much larger than the error in $\tilde{y}_1$, but the error does decrease dramatically nearer the cable (as $|y|$ decreases). From figure 5(b) the error in $\hat{y}_2$ is much smaller than the error in $\hat{y}_1$. (Note the difference in scales in the two figures.) It would appear that the $\hat{y}_2$ data are potentially useful in an automatic system. From figure 5(c) the error in $\hat{\psi}$ is very large. In fact, $\hat{\psi}$ is probably unusable because the errors are large enough in some cases to produce an incorrect algebraic sign for $\hat{\psi}$, a condition which would produce an unstable guidance system.

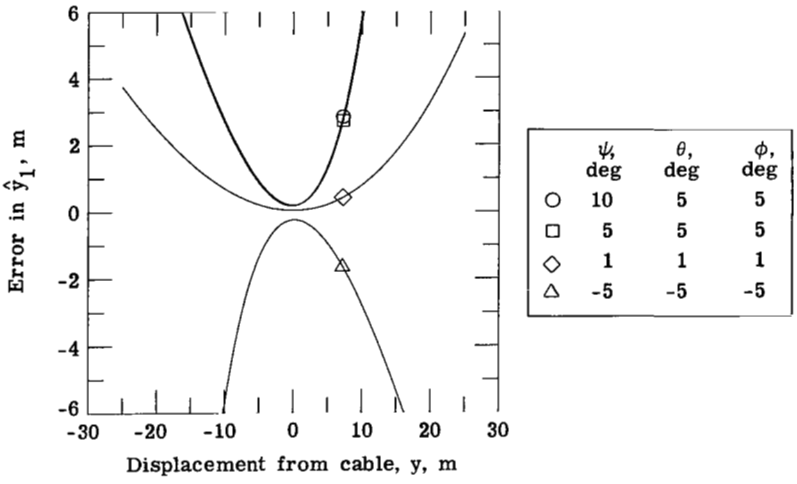

(a) Error in estimate $\hat{y}_1$.

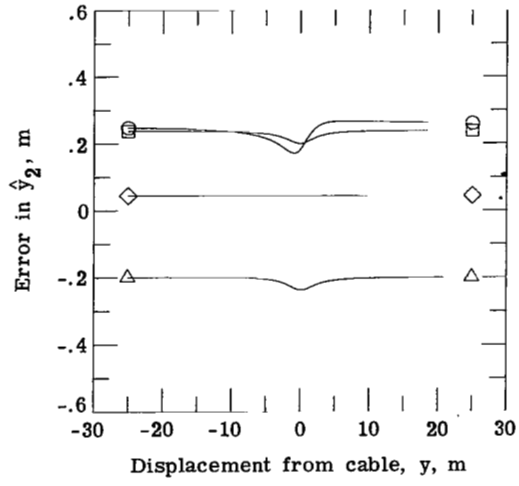

(b) Error in estimate $\hat{y}_2$.

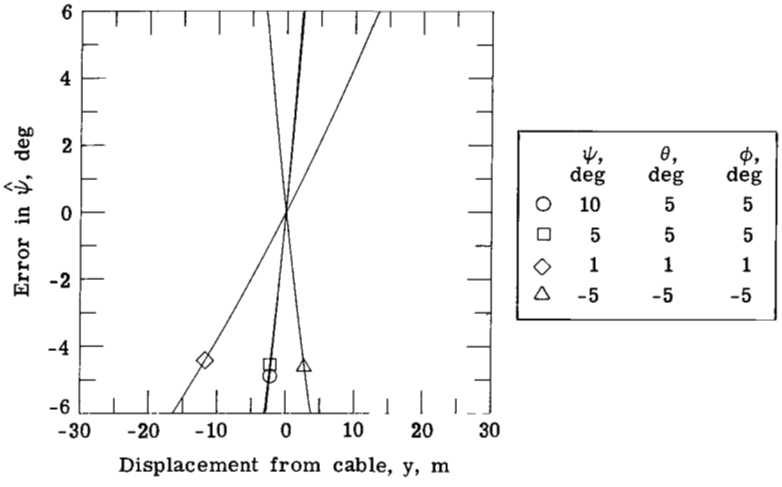

(c) Error in estimate $\hat{\phi}$.

Figure 5.- Error in estimates $\hat{y}_1$, $\hat{y}_2$, and $\hat{\phi}$ due to neglecting aircraft attitude.

EFFECTS OF CLOSED-LOOP GEOMETRY

The previous equations were developed assuming an infinitely long, straight cable. Obviously, a practical installation will not meet these assumptions. The cable will not be infinite and may not be straight, and a return path for the current must be provided.

Consider a cable laid along the runway center line with the return in the form of a closed rectangular loop, as depicted in figure 6. The magnetic intensity produced at point P by a current I in this loop can be found by using the Biot-Savart law to find the incremental intensity $\vec{dH}$ due to a current element $I\,\vec{d\ell}$

and then performing a line integration around the closed loop to get the total intensity $\vec{H}$; that is,

$$\vec{H} = \frac{I}{4\pi} \int_C \frac{\vec{d\ell} \times (\vec{r} - \vec{r}_c)}{|\vec{r} - \vec{r}_c|^3} \tag{19}$$

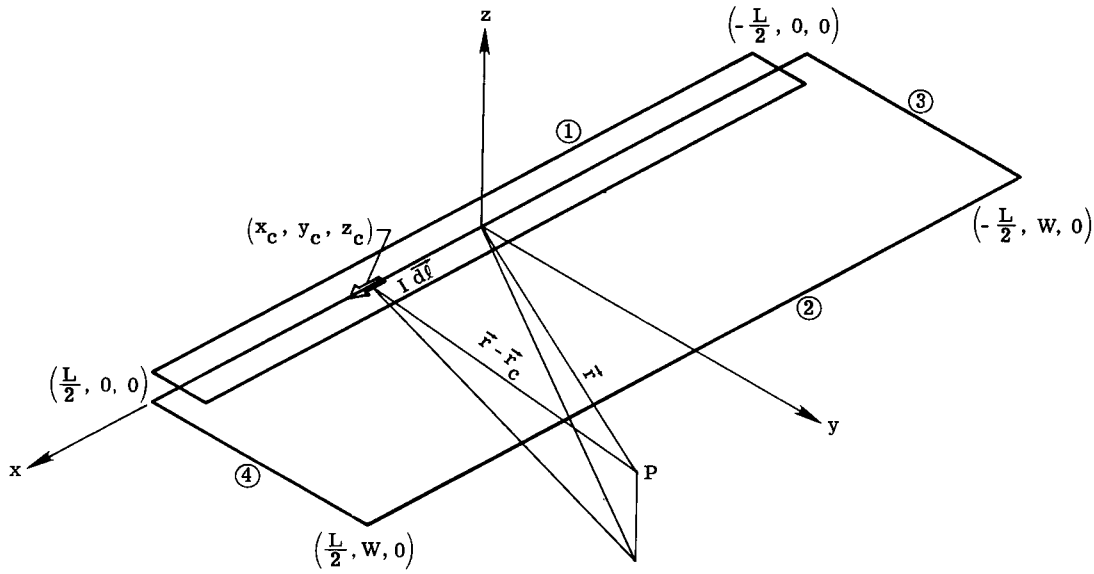

Figure 6.- Geometry of rectangular-loop cable.

The integral in equation (19) can be evaluated in closed form by expressing the integrand in rectangular coordinates and integrating separately over each of the four sides of the rectangle. For side 1 the results are

$$\vec{H}_1 = \frac{I}{4\pi}(-z\hat{i}_y + y\hat{i}_z) \int_{-L/2}^{L/2} \frac{1}{\left[(x - x_c)^2 + y^2 + z^2\right]^{3/2}}\, dx_c$$

$$= \frac{I}{4\pi a_1^2}(-z\hat{i}_y + y\hat{i}_z)\left[\frac{x + \frac{L}{2}}{\sqrt{\left(x + \frac{L}{2}\right)^2 + a_1^2}} - \frac{x - \frac{L}{2}}{\sqrt{\left(x - \frac{L}{2}\right)^2 + a_1^2}}\right] \tag{20}$$

where

$$a_1^2 = y^2 + z^2 \tag{21}$$

Similarly, for sides 2, 3, and 4:

$$\vec{H}_2 = \frac{I}{4\pi a_2^2}\left[z\hat{i}_y - (y - W)\hat{i}_z\right]\left[\frac{x + \frac{L}{2}}{\sqrt{\left(x + \frac{L}{2}\right)^2 + a_2^2}} - \frac{x - \frac{L}{2}}{\sqrt{\left(x - \frac{L}{2}\right)^2 + a_2^2}}\right] \tag{22}$$

where

$$a_2^2 = (y - W)^2 + z^2 \tag{23}$$

$$\vec{H}_3 = \frac{I}{4\pi a_3^2}\left[-z\hat{i}_x + \left(x + \frac{L}{2}\right)\hat{i}_z\right]\left[\frac{y}{\sqrt{y^2 + a_3^2}} - \frac{y - W}{\sqrt{(y - W)^2 + a_3^2}}\right] \tag{24}$$

where

$$a_3^2 = \left(x + \frac{L}{2}\right)^2 + z^2 \tag{25}$$

$$\vec{H}_4 = \frac{I}{4\pi a_4^2}\left[z\hat{i}_x - \left(x - \frac{L}{2}\right)\hat{i}_z\right]\left[\frac{y}{\sqrt{y^2 + a_4^2}} - \frac{y - W}{\sqrt{(y - W)^2 + a_4^2}}\right] \tag{26}$$

where

$$a_4^2 = \left(x - \frac{L}{2}\right)^2 + z^2 \tag{27}$$

The total magnetic intensity is given by the sum of the four components:

$$\vec{H} = \vec{H}_1 + \vec{H}_2 + \vec{H}_3 + \vec{H}_4 \tag{28}$$

Suppose that three orthogonal coils are used to measure the components of the magnetic field produced by the rectangular loop. Using the basic algorithms in equations (18), let the output voltages V_1, V_2, and V_3 be used to compute the estimates $\hat{y}_1$, $\hat{y}_2$, and $\hat{\phi}$. These estimates will be in error because equations (18) were developed assuming that the magnetic field was produced by current in an infinite, straight wire rather than by a closed loop. Let us next examine the magnitudes of these errors as functions of the various parameters.

Variation in Error With y-Position

Figure 7 contains plots of the errors in $\hat{y}_1$ and $\hat{y}_2$ caused by a rectangular loop 3000 m long and 100 m wide. The errors are plotted as a function of y for two values of coil height, $z = 1$ and 6 m. These heights should be near the extremes of heights for coils mounted in the nose of current aircraft. These data are for

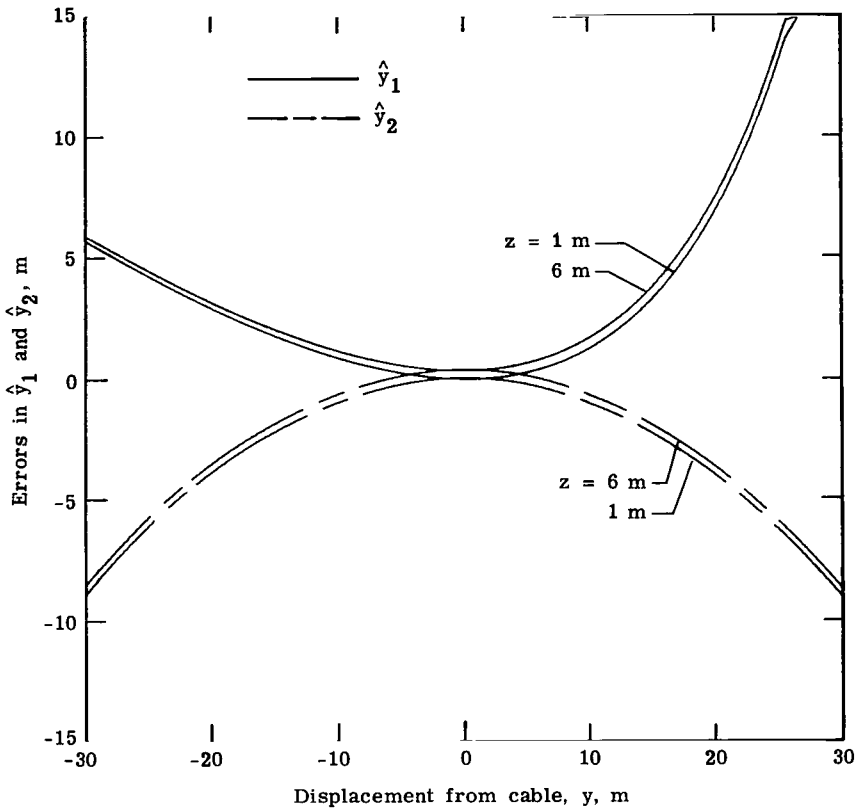

Figure 7.- Error in estimates $\hat{y}_1$ and $\hat{y}_2$ for a 100-m-wide rectangular loop.

$x = 0$; that is, the coil is equidistant from the ends of the loop. The error in $\hat{y}_1$ is larger for positive than for negative values of y because the return side of the cable loop is on the positive side (at $y = 100$ m). There is very little difference in this case in the error for the two different heights. The error in $\hat{y}_2$ is more nearly symmetrical about $y = 0$ than the error in $\hat{y}_1$ and is of the opposite sign. It is worth noting that the error is smallest near the cable ($y = 0$). This is an important factor since the pilot or the automatic control system will be trying to follow the cable. The error in $\hat{\phi}$ in this case is zero because the coils are located at $x = 0$. For all the data in figure 7, the true relative heading is zero ($\phi = 0°$). Results computed for $\phi = 5°$ show errors very close to those in figure 7.

The errors in figure 7 are bias-type errors which cannot be reduced by filtering. However, these errors could be reduced, or even eliminated, by using a nonlinear calibration curve to convert the sensor output voltages to position and heading estimates instead of using the linear relationships from equations (18). Of course, such nonlinear relationships increase the complexity of the system. The calibration curve which accurately relates the sensor output $V_{y_1} = zV_3/V_2$ to the estimate $\hat{\hat{y}}_1$ is shown in figure 8 for a loop width of 100 m. This calibration will be less accurate as the loop width deviates from 100 m.

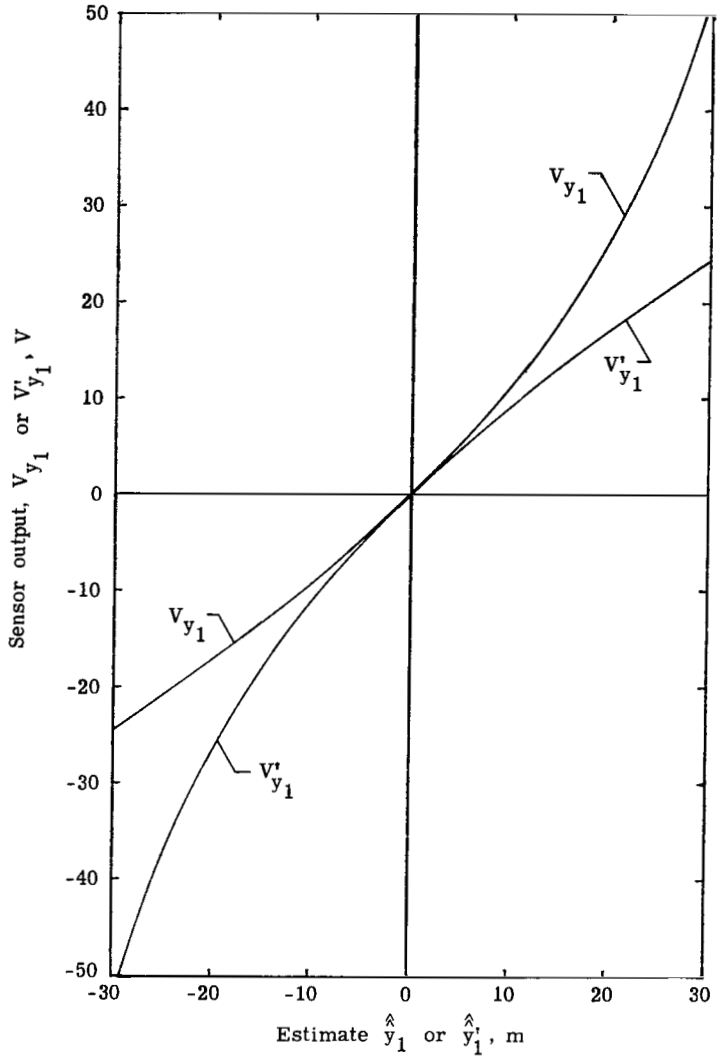

Figure 8.- Nonlinear calibration curves for estimating displacement y for a 100-m-wide rectangular loop.

There is an additional problem to consider. The calibration labeled V_{y_1} in figure 8 and the error curves in figure 7 are for the return wire located at $y = 100$ m and for an aircraft landing in the negative x-direction. Consider an aircraft on the same runway landing in the positive x-direction. For this case, define a new set of coordinates x', y', z', where $x' = -x$, $y' = -y$, and $z' = z$. Now the return wire is located at $y' = -100$ m, and it can be shown that the calibration curve relating the sensor output V'_{y_1} to $\hat{y}'_1$ is the curve V_{y_1} reflected about the origin, as shown in figure 8. Thus, to accurately remove the loop effects with a nonlinear calibration curve requires that the sensor store two curves and that the proper curve be selected for the given landing situation. Alternatively, the sensor could compute the reflection about the origin of a single calibration curve. However, it should be remembered that such accuracy may not be required by an automatic rollout control system. The accuracy requirements must yet be determined via computer simulation and flight testing.

Variation in Error With Loop Width

The errors could also be reduced by increasing the width of the loop and thereby decreasing the effect of the current in the return path. Figure 9 shows the

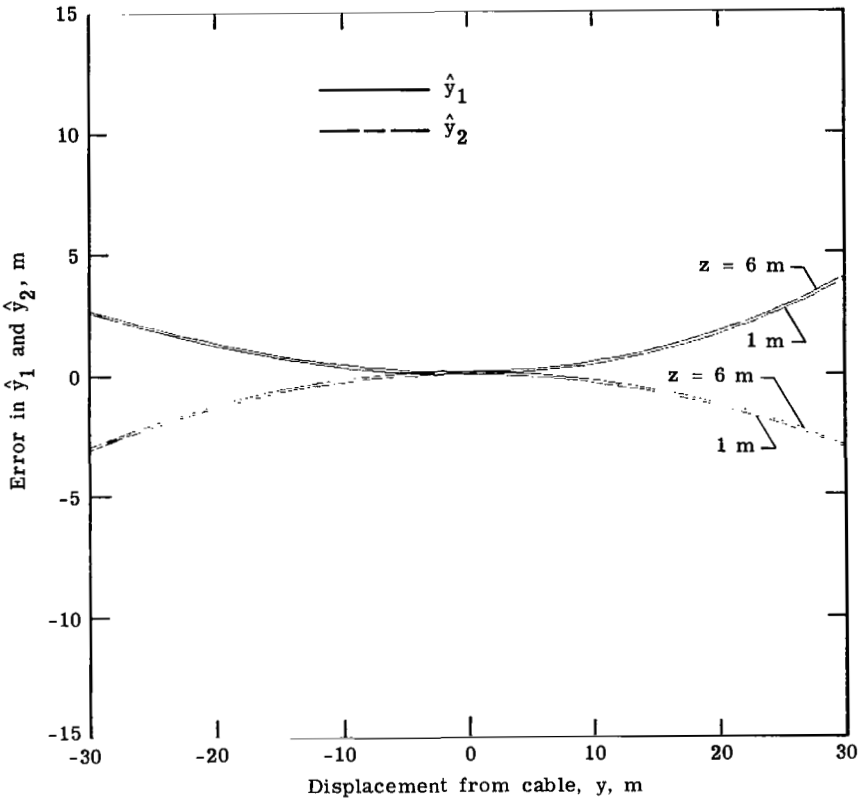

Figure 9.- Error in estimates $\hat{y}_1$ and $\hat{y}_2$ for a 300-m-wide rectangular loop.

same type of errors as figure 7 except that the loop width is 300 m instead of 100 m. As expected, the errors for the 300-m loop are smaller. For example, at $y = 20$ m the error in the estimate $\hat{y}_1$ is 7 m for the 100-m loop and less than 2 m for the 300-m loop. The errors in $\hat{y}_1$ and $\hat{y}_2$ are plotted in figure 10 as a function of loop width W; it can be seen that these errors decrease very rapidly with increasing width for $W < 200$ m. For large values of W (above 600), the rate of decrease in the error becomes very small. The obvious problem in increasing the loop width at a typical airport is the problem of having a place to lay the loop.

Variation in Error With x-Position

The results in figures 7 through 10 are for $x = 0$, and the errors are due primarily to the effects of the return side of the rectangular loop. Near the ends of the loop, errors are also produced by the current in the end. In figure 11 the errors are plotted as a function of the distance along the cable x for two values of y, $y = 5$ and 20 m. The loop is 3000 m by 100 m, and the coil is at a height of 2.5 m. From a value of 7 m at $x = 0$, the error in $\hat{y}_1$ at $y = 20$ m

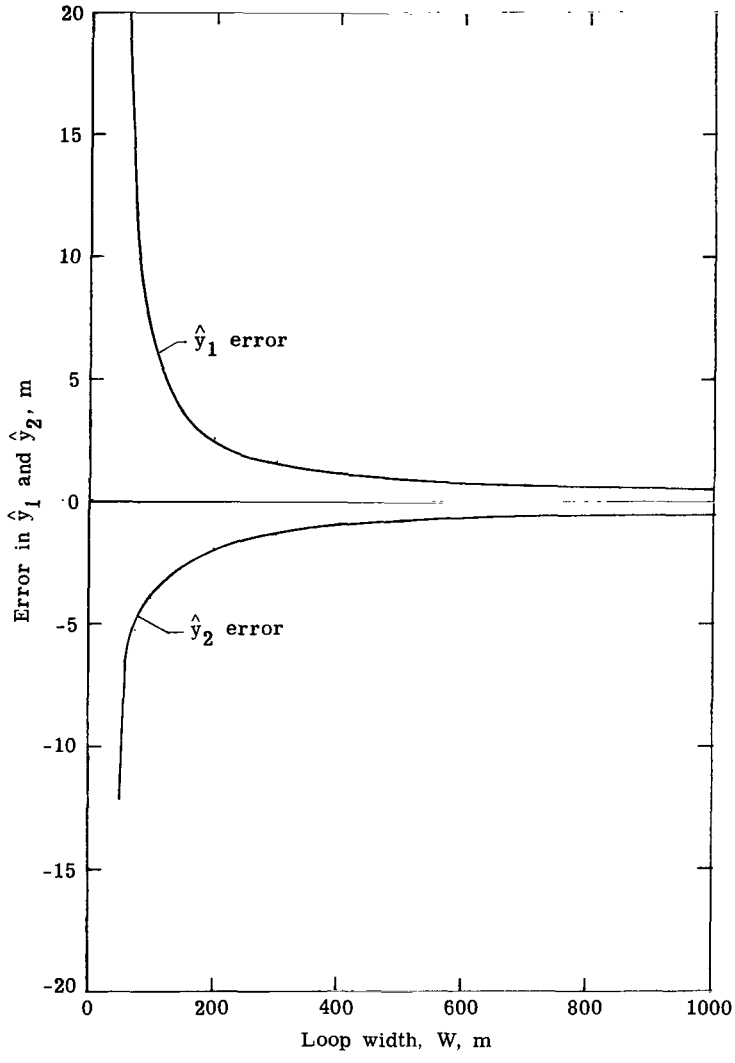

Figure 10.- Error in estimates $\hat{y}_1$ and $\hat{y}_2$ as function of loop width. y = 20 m.

increases to 11 m at a distance 50 m from either end. The effect of the ends on $\hat{\phi}$ is even more pronounced. From a value close to zero (less than 0.1°) along most of the cable, the magnitude of the error in $\hat{\phi}$ increased rapidly within a few hundred meters of the end to a value of 2.5° at 50 m from the end. Unlike the error as a function of y, these end-effect errors cannot be readily reduced by using a nonlinear calibration curve. To reduce end effects, the cable must be laid such that the ends are some 200 to 300 m beyond the active portion of the cable, that is, that part of the cable which the aircraft will follow.

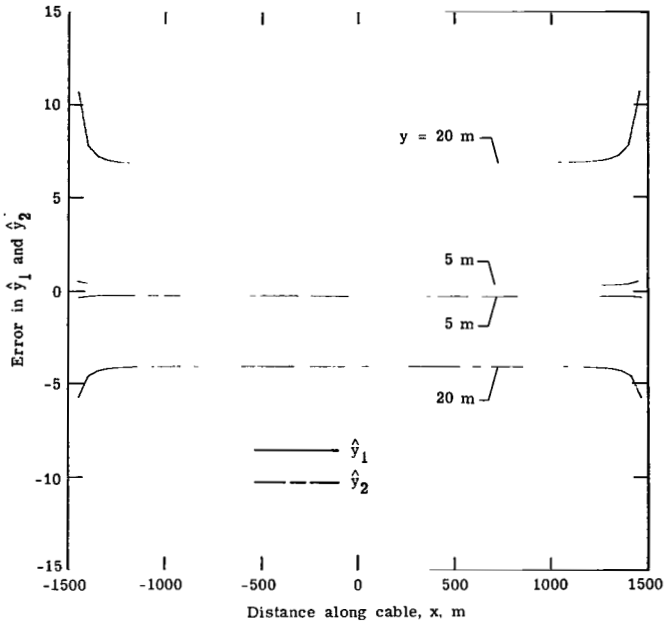

(a) Error in estimates $\hat{y}_1$ and $\hat{y}_2$.

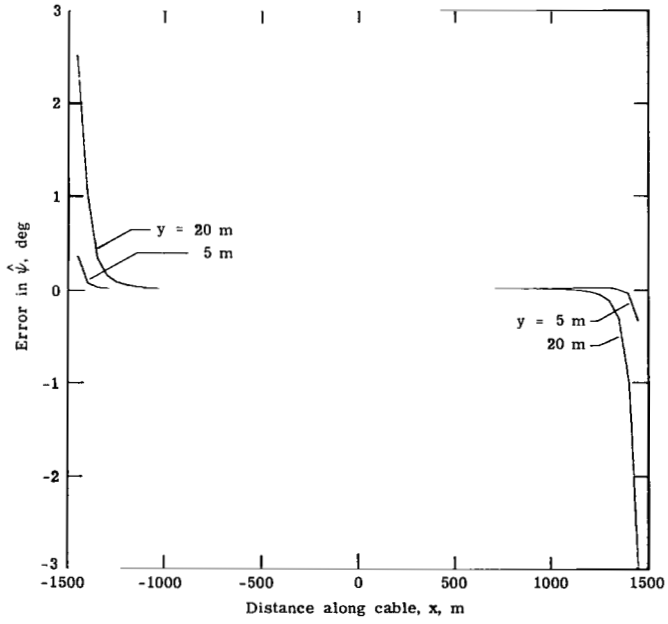

(b) Error in estimate $\hat{\phi}$.

Figure 11.- Error in estimates $\hat{y}_1$, $\hat{y}_2$, and $\hat{\phi}$ due to ends of rectangular loop.

EFFECTS OF TURNOFF GEOMETRY

The rectangular loop is configured to provide guidance in a straight line along one side of the rectangle, such as along the runway center line during rollout. However, it is also desired to provide guidance during turnoff and taxiing. Let us next examine the errors introduced by laying the cable in a runway, turnoff, and taxiway configuration.

Consider the geometry in figure 12. The magnetic intensity at point P is found via line integration of the Biot-Savart law, as in the case of the rectangular loop. The contribution to the total field of the current segments 1 through 5 has the same form as for the rectangular loop. The integrals describing the fields due to the linear and circular arc portions of the turnoff (segments 6, 7, and 8) were not solved in closed form, but rather were evaluated by numerical integration.

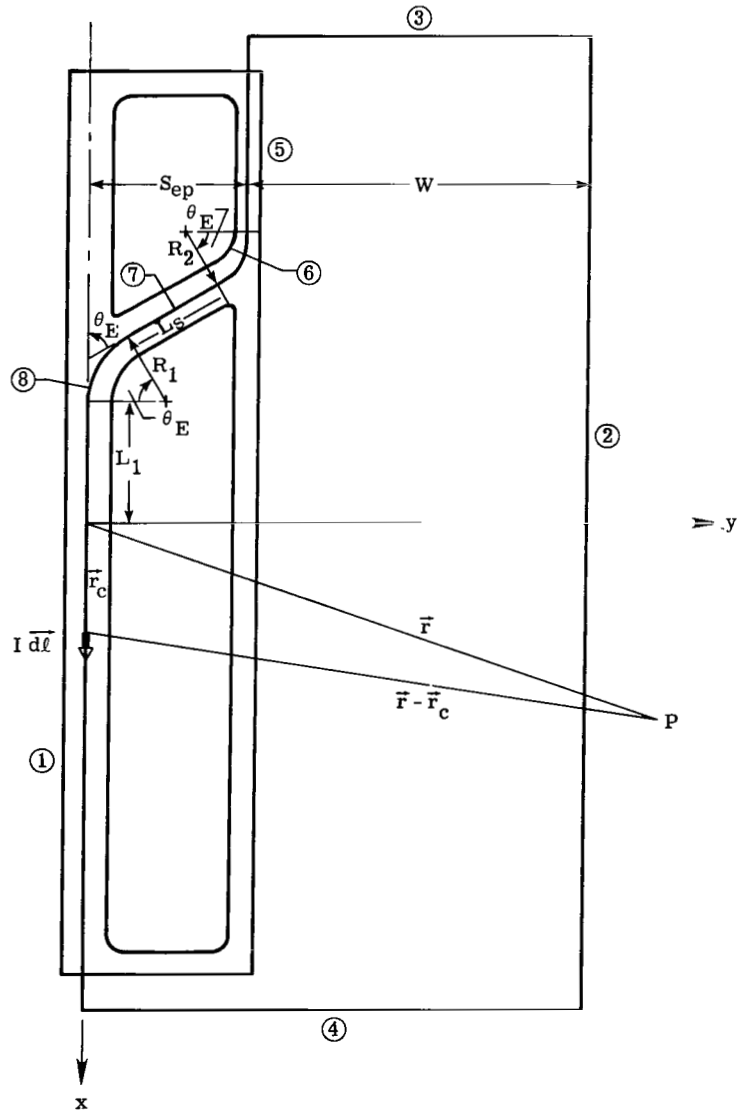

Figure 12.- Loop geometry for turnoff.

These fields were then used to compute the voltages in the coils, which in turn were used to compute the heading estimate $\hat{\psi}$ and the displacement estimates $\hat{d}_1$ and $\hat{d}_2$, using the basic algorithms in equations (18). The variables $\hat{d}_1$ and $\hat{d}_2$ are estimates of d, the linear displacement from the cable in a direction perpendicular to the cable. The variables d, $\hat{d}_1$, and $\hat{d}_2$ correspond to the previously used y, $\hat{y}_1$, and $\hat{y}_2$, but the change in nomenclature is necessitated by the fact that the displacement is not always in the y-direction during turnoff.

The dimensions of a typical runway-turnoff-taxiway configuration are listed in the following table:

Loop length, L, m	3000
Loop width, W, m	100
Runway-taxiway separation, S_{ep}, m	150
Start of turnoff, L_1, m	150
Turnoff angle, θ_E, deg	30
Radius of first turn, R_1, m	550
Radius of second turn, R_2, m	250
Distance between turns, L_s, m	85.6
Height of coils, z, m	2.5

Unless otherwise noted, these dimensions were used in the computations that follow.

Variation in Error With Along-Track Position

The errors produced by the cable geometry were computed as the coils were moved along a path parallel to and at a distance d away from the cable. These errors are plotted as functions of s in figure 13 for values of d = 5 and 20 m. The

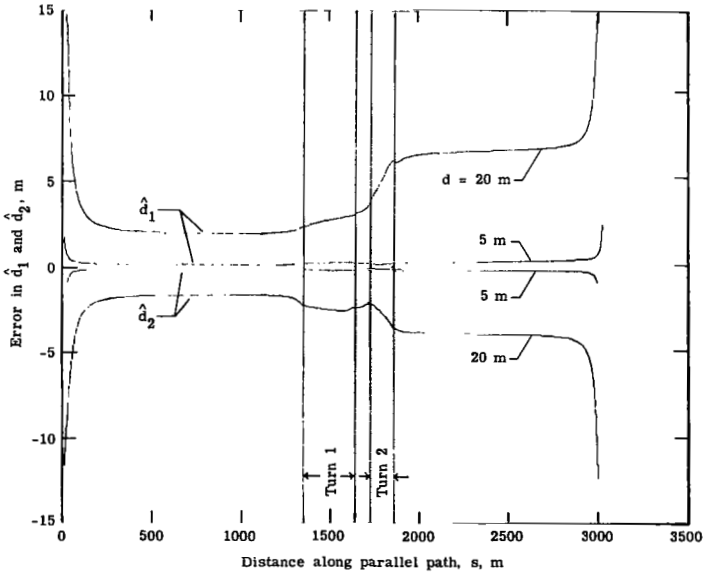

(a) Error in estimates $\hat{d}_1$ and $\hat{d}_2$.

Figure 13.- Error due to turnoff geometry.

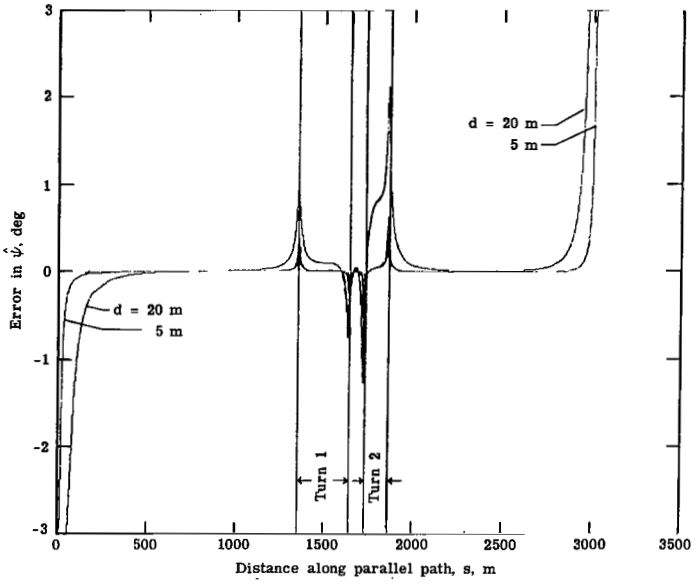

(b) Error in estimate $\hat{\phi}$.

Figure 13.- Concluded.

variable s is the curvilinear distance along the path starting at $x = L/2$ and moving in a negative x-direction; it is analogous to the variable x in the error plots for the rectangular loop.

The following observations can be made about these errors:

1. The errors decrease significantly as the aircraft (coils) approaches the center line (the cable), just as in the case of the rectangular loop cable geometry.

2. The errors in the displacement estimates $\hat{d}_1$ and $\hat{d}_2$ are close to their values for a rectangular loop in areas away from the turns. In the region $1855 \leq s \leq 3000$ the cable is 100 m from the return wire, and the errors in figure 13 are nearly the same as the errors in figure 11 for a rectangular loop 100 m wide. In the region $0 \leq s \leq 1350$ the cable is 250 m from the return wire, and the errors in this region are nearly the same as the errors for a rectangular loop 250 m wide. The error in one region, but not both regions, can be removed by a single calibration curve. Conceptually, multiple calibration curves could be used to reduce the errors in both regions at the expense of increased complexity. Of course, the difference in the errors between the two regions could be reduced by increasing the width of the loop.

3. The errors in the displacement estimates $\hat{d}_1$ and $\hat{d}_2$ vary smoothly in the areas of the turns.

4. In the plot of the error in the estimate $\hat{\phi}$ (fig. 13(b)), spikes occur at the beginning and end of each turn. The magnitudes of these spikes are larger for the larger values of d.

5. In the regions away from the turns, the error in $\hat{\phi}$ is nearly zero, as in the case of the rectangular loop. It is worth noting that the sign of the error in $\hat{\phi}$ at the beginning and end of the turns is such as to provide some lead, or

predictive, information going into and coming out of the turns. The usefulness of this information has not been evaluated.

Variation of Error With Cross-Track Position

In figures 14 and 15 the errors in the estimates $\hat{d}_1$, $\hat{d}_2$, and $\hat{\psi}$ are plotted as functions of d. In figure 14 the path is located at the beginning of the first turn, and in figure 15 the path is located at the beginning of the second turn.

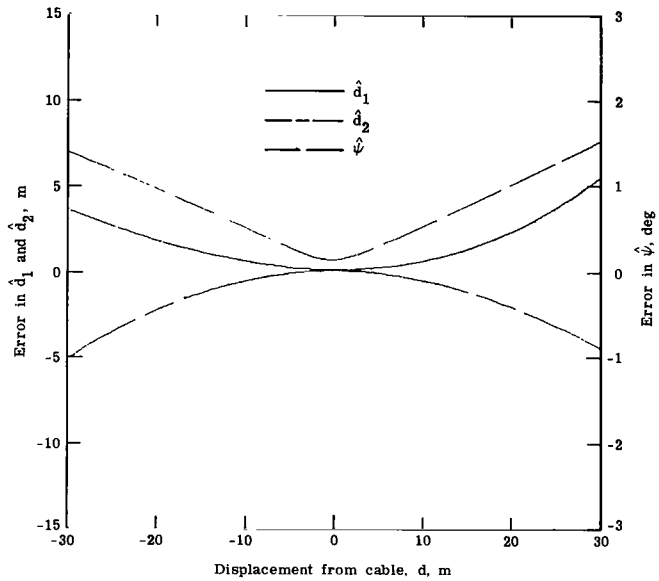

Figure 14.- Error in estimates $\hat{d}_1$, $\hat{d}_2$, and $\hat{\psi}$ at start of first turn.

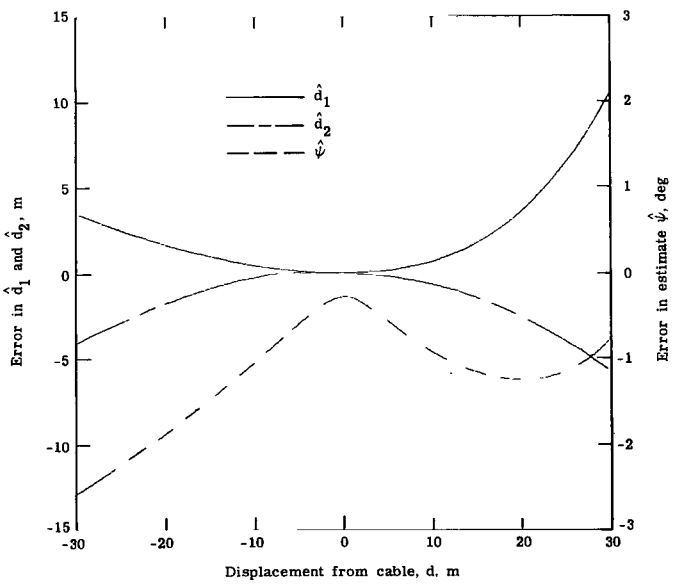

Figure 15.- Error in estimates $\hat{d}_1$, $\hat{d}_2$, and $\hat{\psi}$ at start of second turn.

These locations correspond approximately to the locations of the spikes in the $\hat{\psi}$-error in figure 13(b). We observe that the magnitudes of the errors generally decrease smoothly with decreasing magnitude of d and are minimum near $d = 0$. One exception is the local maximum for the magnitude of the $\hat{\psi}$-error near $d = 20$ m in figure 15.

Variation of Error With Turnoff Angle

Consider now the effect of the turnoff, or exit, angle θ_E on the magnitude of the errors during turnoff. In figure 16 the maximum errors in the estimates during

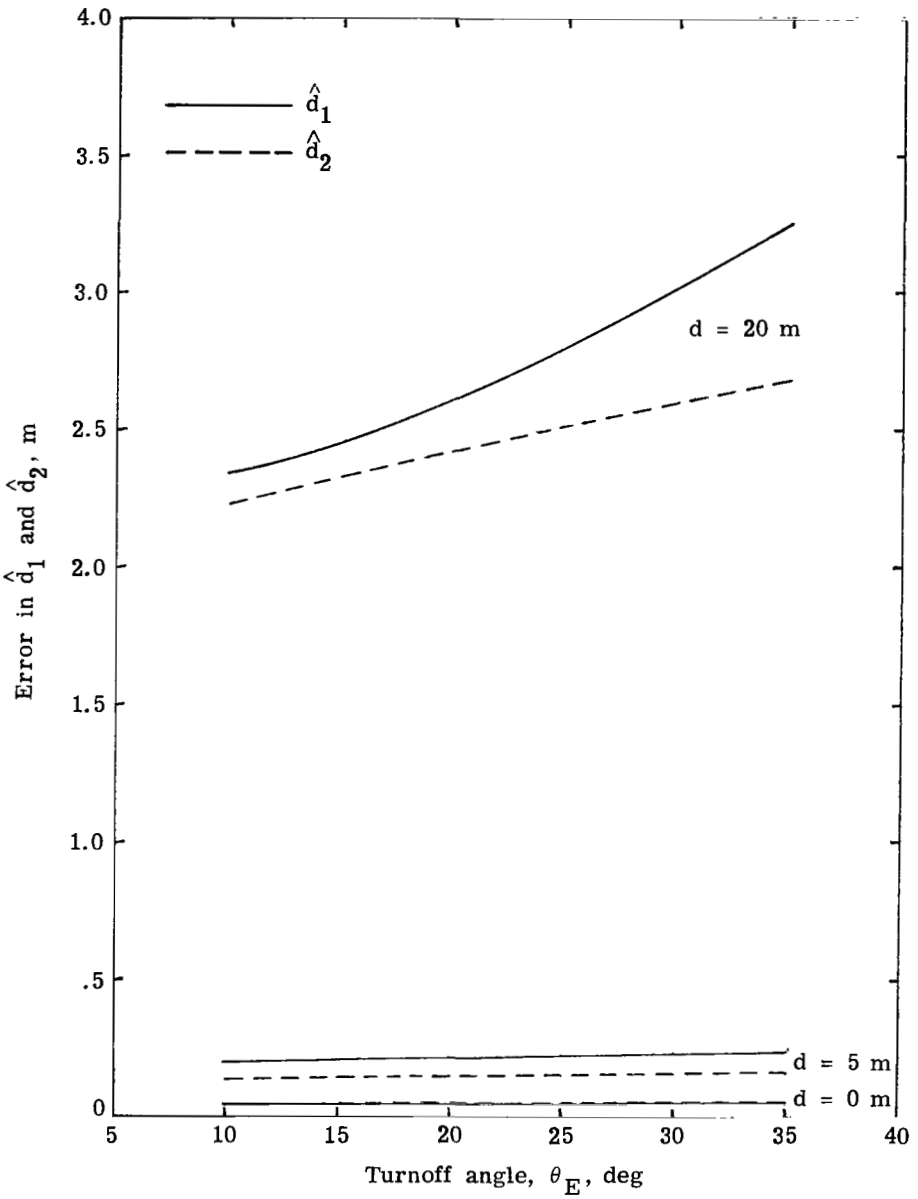

(a) Error in estimates $\hat{d}_1$ and $\hat{d}_2$.

Figure 16.- Maximum error magnitude during turnoff caused by cable geometry as function of turnoff angle.

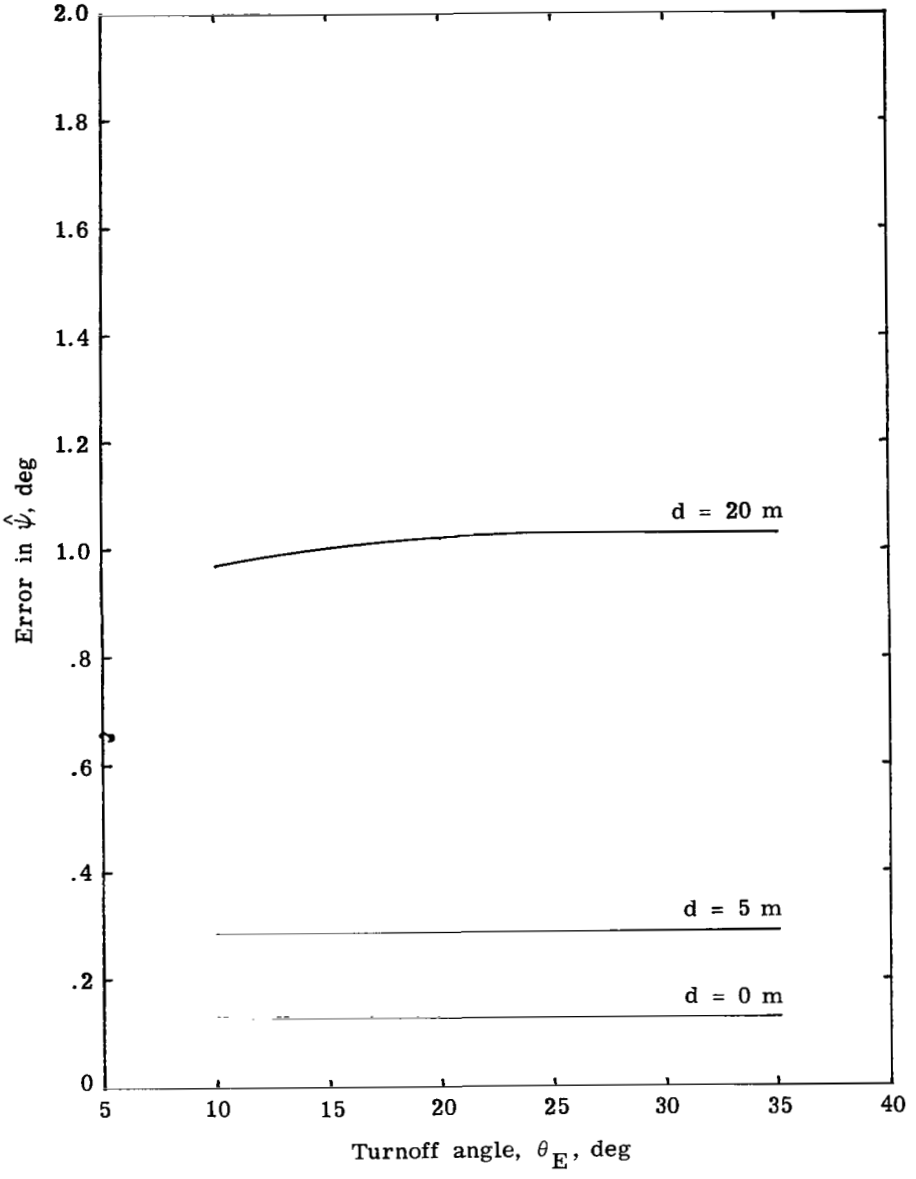

(b) Error in estimate $\hat{\psi}$.

Figure 16.- Concluded.

the first turn are plotted as functions of the exit angle for d = 0, 5, and 20 m. The radius of the first turn is 550 m, as used previously. From these graphs (figs. 16(a) and 16(b)) it can be seen that for positions close to the cable (small values of d), the peak errors are not significantly affected by the exit angle for R_1 = 550 m. At d = 20 m the magnitude of the errors in $\hat{d}_1$ and $\hat{d}_2$ increases slightly with θ_E, but the effect is not large enough to be a determining factor in selecting the exit angle. Larger exit angles are not considered in figure 16 because angles greater than 35.66° are not possible with the given geometry (R_1 = 550 m, R_2 = 250 m, and S_{ep} = 150 m).

Variation of Error With Turnoff Radius

We now consider the effect of the turnoff radius on the errors in the estimates. In figure 17 the maximum error magnitudes are plotted as functions of the turnoff radius for an exit angle of 30°. Maximum error magnitude is meant to be the largest error magnitude encountered as a function of s in the vicinity of the turnoff. From figure 17(a), it can be seen that the maximum errors in the estimates

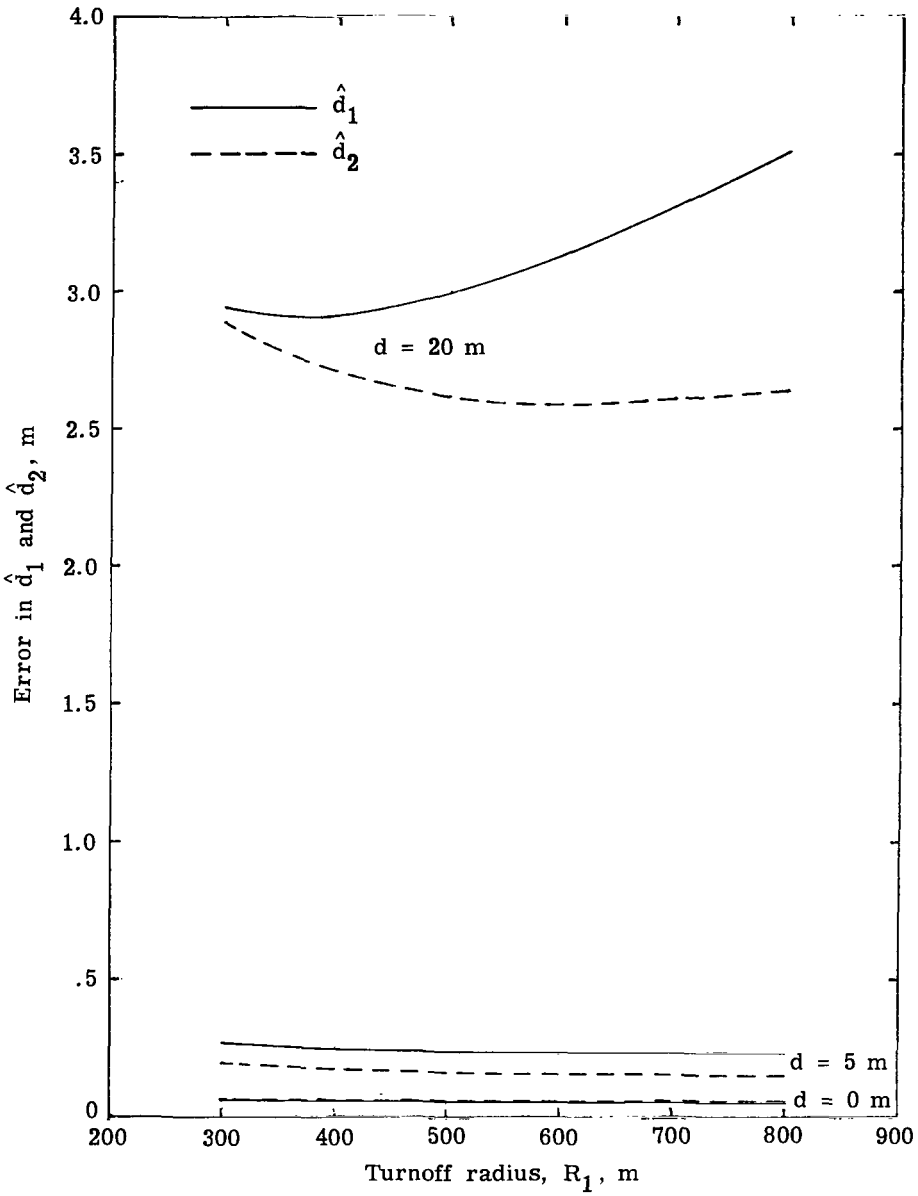

(a) Error in estimates $\hat{d}_1$ and $\hat{d}_2$.

Figure 17.- Maximum error magnitude during turnoff caused by cable geometry as function of turnoff radius.

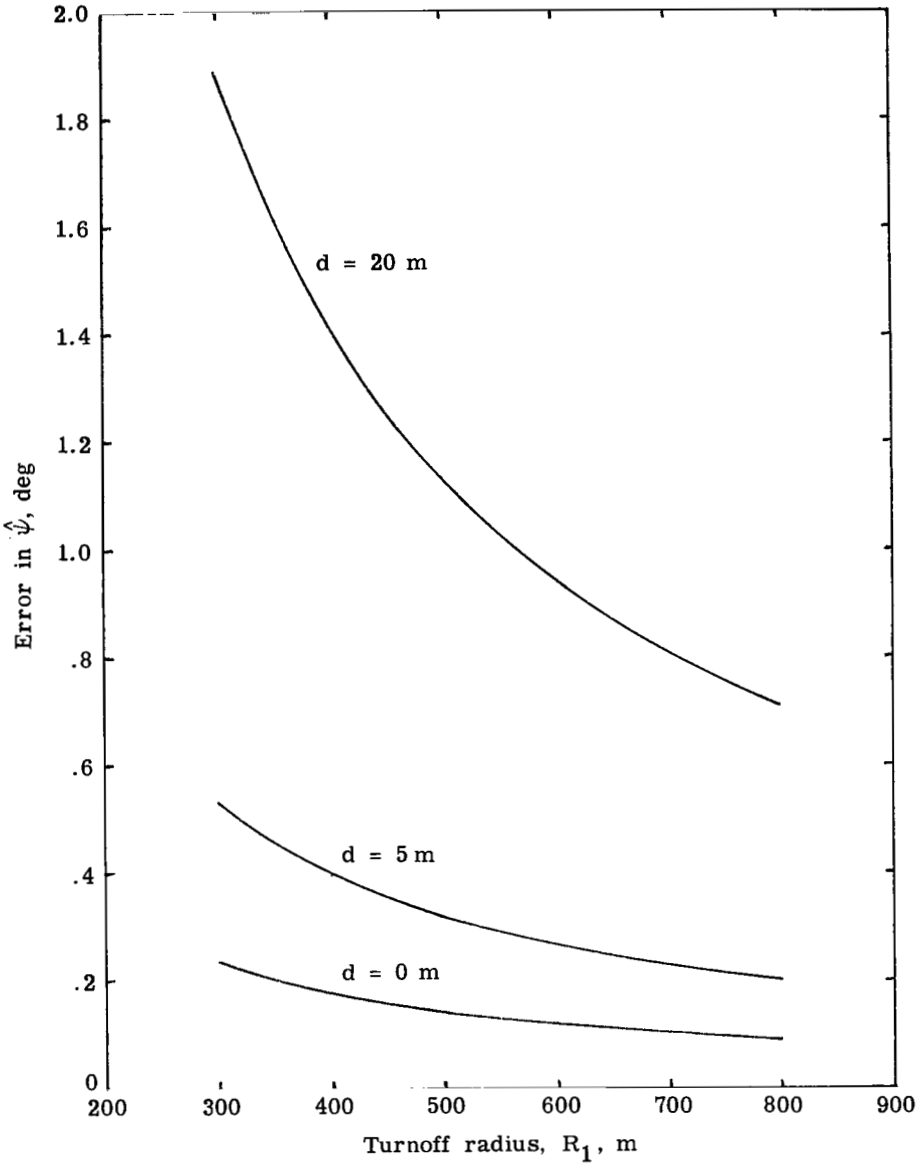

(b) Error in estimate $\hat{\phi}$.

Figure 17.- Concluded.

$\hat{d}_1$ and $\hat{d}_2$ are weak functions of the radius R_1 for small values of d. On the other hand, the peak error in the heading estimate $\hat{\phi}$ decreases with increasing radius, particularly for larger values of d. To minimize the error in $\hat{\phi}$, therefore, R_1 should be made large. Of course, other factors, such as acceleration on the aircraft and available real estate, affect the choice of R_1.

SUMMARY OF RESULTS

This report has examined via a theoretical analysis the errors in a single-wire magnetic leader cable sensor system caused by aircraft attitude and by cable loop geometry. A set of basic algorithms was developed which could be used to compute

y and ϕ (where y is the aircraft lateral displacement from the cable and ϕ is the heading relative to the cable). These algorithms assumed that the cable was configured as an infinitely long, straight wire; also the equations neglected aircraft pitch and roll.

For the estimate $\hat{y}_2$ of the displacement y, it has been shown that the error caused by neglecting aircraft attitude may be small enough to be neglected. However, for the estimate $\hat{\phi}$ of aircraft relative heading ϕ, the error caused by aircraft attitude is large enough that the heading estimate may not be usable. The attitude-induced errors can be significantly reduced by employing the algorithms which include the aircraft attitude angles in the computations using small-angle approximations.

The errors produced by using the basic algorithms when the cable was configured as a closed rectangular loop rather than an infinite straight wire were examined. It was found that these errors decreased in magnitude with decreasing y and reached minimum at or near the cable. The errors increased sharply as the loop width decreased below 200 m; but, if required, these errors could be removed for any given width by using a nonlinear calibration curve for the computation - in other words, by using a more complex algorithm. This calibration curve must be reflected about the origin when heading in the opposite direction on the runway. Also, the errors increased near the ends of the loop, necessitating that the ends be located 200 to 300 m beyond the active, or guidance, portion of the cable. It was found that the turnoff produced additional errors in the estimates, and these errors also decreased in magnitude nearer the cable. Particularly noticeable are the error spikes in the heading estimate at the beginning and ending of the turns. It was found that the maximum magnitudes of the errors in the turnoff were not significantly affected by the turnoff angle for angles in the range of 10° to 35°. The maximum error magnitudes in the estimates of displacement were not strongly affected by the radius of the turnoff for radii between 300 and 800 m. The error in $\hat{\phi}$, however, did decrease significantly with increasing radius for large values of displacement. Although the leader cable concept was originally formulated for the hypothetical case of an infinite straight wire, results of this analysis show that the concept remains viable for a practical closed-loop runway-turnoff-taxiway configuration.

It should be remembered that there are other sources of error, such as ground effects, aircraft metal effects, and sensor noise, which have not been considered in this report. Furthermore, the effect of all errors on aircraft performance during rollout and turnoff, including those analyzed in this report, must be examined via simulation and experimental testing. The sensor performance requirements can then be specified. From these requirements, from the test data, and from the results of the current analysis, the need for aircraft attitude compensation and for nonlinear calibration in the sensor processor can be determined.

Langley Research Center
National Aeronautics and Space Administration
Hampton, VA 23665
March 5, 1982

REFERENCES

1. Hammond, A. F.: Guidance and Control of Aircraft Ground Movement at Airports During Restricted Visibility - A Survey of Requirements and Possible Systems. Tech. Rep. No. 65071, British R.A.E., Mar. 1965.

2. Morgan, H. C.; and England, P.: A Taxi-Guidance System for Aircraft Using a Single Magnetic Leader Cable. Tech. Rep. No. 66065, British R.A.E., Feb. 1966. (Available from DTIC as AD 800 204.)

3. Olson, Karl W.: Wire-Reference Configurations in Vehicle Lateral Control. IEEE Trans. Veh. Technol., vol. VT-26, no. 2, May 1977, pp. 161-172.

4. Mukhopadhyay, Asok K.; and Dobrotin, Boris M.: Time Response Simulation of the Guidance and Control System of an Automatically Steered Wire-Following Vehicle. ITC/USA/'79 International Telemetering Conference, Volume XV, Inst. Soc. America, 1979, pp. 85-94.

5. Pines, S.; Schmidt, S. F.; and Mann, F.: Automated Landing, Rollout, and Turnoff Using MLS and Magnetic Cable Sensors. NASA CR-2907, 1977.

6. Pines, S.; and Hueschen, R. M.: Guidance and Navigation for Automatic Landing, Rollout, and Turnoff Using MLS and Magnetic Cable Sensors. A Collection of Technical Papers - AIAA Guidance and Control Conference, c.1978, pp. 393-406. (Available as AIAA Paper 78-1296.)

7. Pines, Samuel: Terminal Area Automatic Nagivation, Guidance, and Control Research Using the Microwave Landing System (MLS). Part 1 - Automatic Rollout, Turnoff, and Taxi. NASA CR-3451, 1981.

1. Report No.	2. Government Accession No.	3. Recipient's Catalog No.
NASA TP-1978		

4. Title and Subtitle	5. Report Date
EFFECTS OF CABLE GEOMETRY AND AIRCRAFT ATTITUDE ON THE ACCURACY OF A MAGNETIC LEADER CABLE SYSTEM FOR AIRCRAFT GUIDANCE DURING ROLLOUT AND TURNOFF	April 1982
	6. Performing Organization Code 534-04-13-54
7. Author(s) W. Thomas Bundick	8. Performing Organization Report No. L-14975
	10. Work Unit No.
9. Performing Organization Name and Address NASA Langley Research Center Hampton, VA 23665	11. Contract or Grant No.
	13. Type of Report and Period Covered Technical Paper
12. Sponsoring Agency Name and Address National Aeronautics and Space Administration Washington, DC 20546	14. Sponsoring Agency Code

15. Supplementary Notes

16. Abstract

A theoretical analysis of a single-wire magnetic leader cable system for aircraft rollout and turnoff guidance has been performed to determine the errors produced by the leader cable installation geometry and aircraft attitude. It was found that errors in the measurement of lateral displacement from the cable are smaller than errors in the measurement of aircraft heading and that both errors are smallest at or near the cable.

17. Key Words (Suggested by Author(s))	18. Distribution Statement
Magnetic leader cable Automatic turnoff Aircraft guidance Avionics Rollout Aircraft control systems	Unclassified - Unlimited Subject Category 04

19. Security Classif. (of this report)	20. Security Classif. (of this page)	21. No. of Pages	22. Price
Unclassified	Unclassified	30	A03

For sale by the National Technical Information Service, Springfield, Virginia 22161

NASA-Langley, 1982

National Aeronautics and Space Administration

Washington, D.C. 20546

Official Business

Penalty for Private Use, $300

THIRD-CLASS BULK RATE

Postage and Fees Paid
National Aeronautics and Space Administration
NASA-451

U.S.MAIL

NASA

POSTMASTER: If Undeliverable (Section 158 Postal Manual) Do Not Return